Results of Slat CPC Prototype Test for ALICE Dimuon Spectrometer

M. Boudjemline, H. Carduner, D. Charrier, J.P. Cussonneau, M. Dialinas [a],
Ch. Finck, S. Fresneau, P. Lautridou, L. Luquin, P. Pichot, D. Thers [a],
A. Baldisseri, H. Borel, E. Dumonteil, J. Gosset, D. Jourde [b],
J.C. Lugol, F. Orsini, Y. Penichot, J.P. Robert, F. Staley [b],
M. Arba, S. Basciu, C. Cicaló, A. De Falco, D. Marras, A. Masoni [c],
S. Panebianco, G. Puddu, S. Serci, E. Siddi, L. Tocco, M. Tuveri, G. Usai [c],
G. Chabratova [d],
M.P. Comets, P. Courtat, Ch. Diarra, B. Espagnon, D. Guez, Y. Le Bornec [e],
M. Mac Cormick, J.M. Martin, S. Rousseau, T. Sinha, N. Willis [e],
V. Nikulin [f]

[a] *SUBATECH, Nantes, France*
[b] *DAPNIA/SPhN,CEA-Saclay, France*
[c] *INFN and University, Cagliari, Italy*
[d] *JINR, Dubna, Russia*
[e] *IPN, Orsay, France*
[f] *PNPI, Gatchina, Russia*

Abstract

A full size Slat prototype of a Cathode Pad Chamber has been tested in a π^- beam at the CERN PS in October 2001. The results of these tests are presented in this note. In particular, a study of the spatial resolution and the efficiency has been made: the spatial resolution is found to be around 80 μm while the efficiency is greater than 96 %.

1 Introduction

The three rear stations of the ALICE dimuon spectrometer will be built with the slat concept proposed in the Technical Design Report (TDR) [1]. In this case the chamber is made by vertically assembling some horizontal modules called "slat" of different lengths to cover the acceptance of the spectrometer. Each slat consists of an anode plane with vertical wires and two cathode planes made with Printed Circuit Board (PCB) glued onto a sandwich structure. The use of light composite material allows to minimize the weight and the average radiation length of the chamber (< 2 % of X_0). Moreover, by reducing the total length of the anode wires, the stress can be minimized, the mechanical structure is simplified and reliability is increased. In this design the wires are not soldered but glued with epoxy resin in order to avoid chemical induced failure of the wires. The slat is finally closed with RTV glue, to ensure the gas tightness and the rigidity of the detector but remains able to open. The cathode pad planes and the corresponding connectors for the Front End Electronics (FEE) are made using the same double faced PCB in oder to minimize the length of the strips. On the other side of the PCB, the connecting lines of the read out system are located, taking information from the strips by a metalized hole and bringing it to the connector of the front end electronic card. We will report in this note the results obtained concerning the efficiency and the spatial resolution of a full size slat prototype. The dimension of the active area of this detector is 2400×400 mm^2, corresponding to the biggest slat of this design.

2 Prototype Description

The main idea of the slat design is to remove all metallic parts of the detector except the anode wires and the copper of the PCB. Consequently, only composite and synthetic materials are used in the assembly process of the slat. The anode plane is made with 20 μm diameter Tungsten Rhenium (97 %W + 3 % Re) wires glued with epoxy resin on a Noryl (PPO) spacer. The small length of the anode wires (40 cm, type: LUMA861/60) allows to reduce the mechanical strength to about 40 g. The positioning (pitch and gap) of the wire is achieved by a V-shaped groove. The electric connection between wires is ensured by copper strip/conductive epoxy of 4 mm width. The anode wire pitch and the anode to cathode distance are 2.5 mm. Thus the two cathode planes are separated by a 5 mm gap filled with Ar-CO_2 (80:20) gas mixture. Each cathode plane is glued on a 8.4 mm thick carbon sandwich panel made with two 200 μm carbon skins separated by a 8 mm Nomex honeycomb layer. Each carbon skin is made of two 100 μm thick high modulus carbon fiber skins assembled perpendicularly to obtain pseudo isotropic properties.

To minimize the electronic noise, the capacitance has been decreased by gluing a 0.25 mm Nomex foil between the PCB and the carbon sandwich. Figure 1 shows a schematic view of this prototype. The cathode pads are printed on 400 μm thick FR4 board. The dimension of the modular cathode active area is $(6\times400)\times400$ mm^2, and the total size of a standard PCB is 400×580 mm^2. Thus the Front End Electronic cards, named MANU345, can be plugged at the edge of the detector as shown in Fig. 1. The size of the pads is 25×5 mm^2 in the bending plane (i.e. when the longest dimension of the pad is perpendicular to the anode wire) and 7.14×25 mm^2 in the non-bending plane. The amount of copper is reduced as much as possible by using a double sided 9 μm layer on FR4 substrate. Due to the etching process, the total copper thickness is around 20 μm but not well known. Measurements of the real thickness of the copper will be achieved soon. The read-out lines connected to the cathode strips through vias are 180 μm wide and their lengths range from 9 mm to 199 mm. The minimum distance between two read-out lines is 150 μm. More details can be found in Ref. [2].

3 Experimental Setup

The slat prototype was tested in the T10 area of the PS complex at CERN. The beam used was 7 GeV/c momentum π^-. The tracking system was made by 5 X and 5 Y silicon strip detectors. The width of the strips is 50 μm giving a resolution around 15 μm. Three of them were placed in front of the CPC prototype and two behind. Each silicon detector has 768 channels, read by a dedicated electronic based on multiplexed chips. The CPC front end electronics (FEE) is equipped with GASSIPLEX 3-07 [3]. For the final electronics, the GASSIPLEX chips will be replaced by the MANAS chips produced in India. Fig. 2 describes the setup with the relevant position of each element. The trigger was made by a coincidence between a cross of two scintillators placed in front of the first silicon detector and a second one placed after the last silicon layer (this defined a small area 20×20 mm^2 and only tracks parallel to the beam were accepted). The trigger rate was not limited by this small area but by the DAQ system and the number of channels to read. The frame supporting the chamber was able to move along the two directions perpendicular to the beam (X and Y). Thus a scan of the chamber was possible, as well as a rotation of the chamber.

4 Noise Characteristics

The measured level of noise ranges between 0.9 and 1.1 ADC channels (Fig. 3), which corresponds to 1150 to 1400 electrons (0.18 fC and 0.22 fC). This noise level has been achieved by linking all the planes (panels' carbon skins and PCB ground) to a common ground, floating during the test beam and not connected to the general ground of the experimental hall. The total noise of the device is the sum of two contributions. The first one is the intrinsic noise level of the FEE ($\sim$ 500 electrons) and the second one is due to the overall capacitance seen by the GASSIPLEX. As shown in Fig. 4, the noise level is little dependent on the length of the read-out strips connecting the pads to the electronics.

5 Analysis Method

5.1 Reference tracks

As mentioned in the above section, the five silicon detectors are used to determine the trajectory of the particle. A straight line fit is performed imposing the condition that all 5 planes fired in each direction, with a 4σ online pedestal subtraction. Only the cluster with the maximum charge is considered for each plane. Taking into account multiple scattering (1 % X_o for the CPC, 3% X_o for the 10 Silicon planes), and the error on the track fit, this setup allows to have reference tracks with an accuracy around $\sigma \sim 40$ μm.

5.2 Cluster finding in the Slat CPC

The first step of the chamber analysis is to find clusters among fired pads. The cluster finding is done independently in the bending and non bending cathode planes. The procedure finds all the clusters of the slat. Then only the cluster with maximum charge (considered as the beam signal) is kept to determine the position of the cluster.

5.3 Resolution and reconstruction efficiency definitions

Each track is extrapolated to the Z-position of the chamber, giving the corresponding X, Y position of the particle through the chamber.

The spatial resolution of the slat is derived from Gaussian fits of the residuals, defined as the distance between the extrapolated tracks and the position measured in the chamber. Several methods have been applied to determine the resolution of the slat (see next section). The resolution is not corrected for multiple scattering of the pions.

In the following the reconstruction efficiency is given by the ratio of the number of clusters found in the chamber and the reconstructed tracks from the silicon detectors, for a window of residuals less than 1 mm.

The absolute tail is defined as the relative amount of events outside the window $\pm$ 300 μm (within the $\pm$ 1 mm range), with respect to the center of the residual distribution.

For this analysis, an off-line pedestal subtraction of 3σ has been chosen for the slat signal.

5.4 Position reconstruction with a Mathieson fitting procedure

Two different methods were studied for the reconstruction of the particle position on both cathodes independently:

- The first one is a simple center of gravity calculation from all induced charges in a cluster. This method implies the usual correction depending on the distance of the particle to the central pad position (i.e: the pad crossed by the particle). The same kind of correction has been applied to all the clusters, even if it depends on the number of pads it contains.
- The second method is a full two dimensional fit to the charge distribution with a realistic function, namely a Mathieson charge distribution. As the CPC is asymmetric in X/Y, this distribution is defined by two parameters: K_{3x} and K_{3y}. Their values are only defined by some characteristics of the detector's geometry, namely: the anode-cathode distance, the anode wire pitch and the anode wire radius. In our case, the values for the parameter $\sqrt{K_3}$ are given in Table 1 (see Ref. [4,5]).

$\sqrt{K_{3x}}$	$\sqrt{K_{3y}}$
0.761577	0.714143

Table 1: $\sqrt{K_3}$ in the X and Y directions

In its simplest version (one cluster), the Mathieson fitting algorithm con-

sists of minimizing the following χ^2:

$$\chi^2(x_{rec}, y_{rec}) = \sum_i \{(q^i_{meas} - q^i_{Math}(x_{rec}, y_{rec}))/\sigma^i_{meas}\}^2$$

where q^i_{meas} is the measured individual charge of the pads in one cluster and $q^i_{Math}(x_{rec}, y_{rec})$ is the Mathieson function of the reconstructed position (x_{rec}, y_{rec}). A same noise ($\sigma^i_{meas} = 1$ ADC channel) on each pad is assumed in the function $\chi^2(x_{rec}, y_{rec})$. The minimization is based on the Minuit package.

Both methods lead to about the same performances but the Mathieson fit benefits from being less sensitive to the possible variation of the anode-cathode distance and it does not require additional corrections. Moreover the fit to a known charge distribution becomes necessary in the high density environment of ALICE where close hits have to be disentangled. The results shown in this paper have been obtained with the Mathieson fit method.

6 High voltage dependence

Several high voltages were applied in the range 1600 to 1825 V to the third section, among six available, of the slat. The beam spot illuminated a region centered at the position X=51, Y=16 cm with respect to the middle of the chamber over an area of about 2 cm^2. No calibration of the electronics channels has been performed during this analysis since it was not available on the current version of MANU345.

Fig. 5 shows the evolution of the total cluster charge as a function of the high voltage for the bending plane. The most probable value of the Landau fit of the distribution is plotted on this figure. The conversion into charge units assuming an amplification of the GASSIPLEX of 3.6 mV/fC and an ADC range of 3 V for 4096 channels gives an absolute gain of the order of few 10^4 at 1700 V. The cluster charge, as expected, follows an exponential law with the increasing electric field. A typical total charge spectrum per cluster is shown in Fig. 6.

Figure 7 shows the resolution for different fitting procedure and the amount of absolute tail as a function of the applied high voltage. Square symbols represent the results obtained with a simple Gaussian fit (open symbols were obtained with error bars of the fit weighted to 1 to better fit the peak) and star symbols indicate the double Gaussian fit procedure. One can notice that the results are compatible within a range of 10 μm, which could be considered as an estimation of the resolution precision. The spatial resolution displays a long plateau for voltages ranging from 1675 to 1750 V. A typical residual

spectrum for the bending plane is depicted in Fig. 8 for 1725 V. The resolution achieved is better than $\sigma = 80$ μm and the amount of events in the tail of the distribution is less than 4 % for the bending plane. To take into account the tails of the distribution, the RMS value is also shown for comparison (crosses in Fig. 9). An RMS value of 140 μm is obtained up to 1750 V. Above 1750 V, a deterioration of the spatial response function of the slat is visible not only in the resolution but also in the amount of absolute tail. This deterioration is particularly significant for the RMS value, which grows up to 220 μm by 1825 V. This effect is partially due to saturations of the electronic (GASSIPLEX pre-amplifier saturation), revealed by Fig. 9. Indeed, the percentage of saturated clusters (i.e. clusters with at least one saturated pad) grows with the applied high voltage (see Fig. 9 bottom). As expected the RMS value is obviously more affected than the resolution by the saturation effect (see Fig. 9 top).

Fig. 10 bottom presents the average number of pads per cluster in the bending direction, which is 3 for the plateau region and increases abruptly above 1750 V. The top picture details the relative weight of the different pad configurations. Beyond the plateau region, configurations with more than 3 pads become predominant and the resolution is poorer (see Fig. 11). This can partly explain the sudden deterioration of the resolution at high voltages from 1775 V.

The reconstruction efficiency for a $\pm$ 1 mm cut on the residual exhibits a rather flat behavior over the given range (see Fig. 12 dot symbol). The mean value of this efficiency is about 96 %. The corresponding efficiency for a $\pm$ 240 μm (3 σ) cut is 92% and decreases above 1750 V due to the tails, as one can see on Fig. 12 (triangle symbol). Of course, the detection efficiency is very good, more than 99.9 %. As a conclusion, the gain could be decreased without any loss of the performances of the chamber, to a running condition high voltage around 1675 V.

Secondary clusters, i.e. in a same event a cluster in addition to the beam signal cluster, have been observed and considered as a small cross-talk signal between read-out strip lines. Indeed, in the y direction (parallel to the anode wire) in the bending plane, the read-out strips are alternated, meaning a short read-out strip for one pad corresponding to one electronic channel followed by a long read-out strip for the following electronic channel corresponding to another pad. Therefore a peak signal is clearly seen on Fig. 13 (left), representing the hits coming from the beam and a cross-talk signal at an other position. Only 4-5 % of the hits are concerned by cross-talk at 1750 V, decreasing to about 0.1 % at 1650 V. When weighting by the charge, only the beam signal emerges (Fig. 13 (right)). The ratio between the beam cluster charge and the cross-talk cluster charge is more than 100. A simulation of the situation when the read-out strips are not alternated, i.e. when beam signal and cross-talk signal contribute to the same cluster, has shown that neither the resolution

is affected (about 3 μm for a 100 charge ratio) nor the efficiency, stable at 96 %. Indeed, the latter solution was tested in the past, giving the same kind of resolution (80 μm) for a comparable noise level. The alternated read-out strips solution was, in purpose, tested to possibly see a cross-talk effect. In the future PCBs'the read-out strips will not be alternated.

7 Angle dependence

Measurements have been done tilting the slat in the plane defined by the beam axis and the wires, from the nominal perpendicular position with respect to the beam axis to angles up to 10^o in steps of 2^o. Results are shown in Fig. 14 for the bending plane. The cluster charge is not affected by this rotation whereas a significant deterioration is seen in the resolution and in the amount of events in the tail of the distribution ($\pm$ 3 σ). This is related to a larger spread of the induced charge over the wire. At 10^o a resolution of σ = 150 μm is reached with an 8 % absolute tail.

As expected, rotating the chamber around the anode wire axis (up to 10^o) does not affect the response of the chamber. No change either in the resolution nor in the efficiency is observed (see Fig. 15).

8 Position dependence

Several positions of the slat have been illuminated with the beam on section 3 and in between sections 2 and 3. The results are shown in Fig. 16 for the cluster charge, efficiency, resolution, and amount of tail. The numbers in parenthesis represent the coordinates, in cm, with respect to the center of the slat. A variation of more than 20 % in gain is seen, no significant influence is observed in terms of efficiency or space resolution. These results are again obtained without electronic calibration.

9 Non-bending plane

As observed in the bending plane, a significant degradation of the RMS value is observed for high voltages above 1750 V in the non-bending plane (see Fig. 17).

Fig. 18 shows a typical residual spectrum obtained at 1725 V, the RMS of the distribution is close to 470 μm at the equivalent efficiency as the one

in the bending plane, much better than the 2 mm required for the dimuon spectrometer.

No angular dependence was found in the response of the non-bending plane.

A slight variation of $\sim$ 5 % of the RMS value of the resolution is measured for the non-bending plane over different positions.

10 Charge correlations

The correlation factor of the charge between the two planes has been found to be higher than 94 %, implying of a good charge sharing between the planes (see Fig. 19). In the same figure, the cluster charge ratio between the two planes gives an RMS value of 0.13 (without calibration).

11 Conclusions

The test of this full sized prototype validates the slat concept, as well as the FEE (MANU 345 fitted for GASSIPLEX 3-07). Some improvements have to be made but the requirements are fulfilled. The one ADC channel of noise (1250 electrons) achieved allows a resolution around 80 μm at normal incidence, with an efficiency better than 96 % at $\pm$ 1 mm. These results are obtained without any electronic calibration and any correction on the multiple scattering effect estimated to about 40 μm. They fulfill the dimuon arm requirement of 100 μm resolution in the bending plane.

12 Acknowledgment

PNPI and JINR work has been supported in part by grant INTAS 00-00538.

References

[1] TDR Dimuon Forward Spectrometer CERN/LHCC **99-12** (1999), Addendum Dimuon Forward Spectrometer CERN/LHCC **2000-046** (2000).

[2] Internal Note: http://www.ca.infn.it/~cicalo/muon/assembly.ps.gz (2002).

[3] J.C Santiard, K. Marent, ALICE-PUB-2001-49.

[4] E. Mathieson N.I.M. A **270** (1988) 602 and reference therein.

[5] Liliane Kharmandarian, Thesis IPNO-T **00-02** (1999).

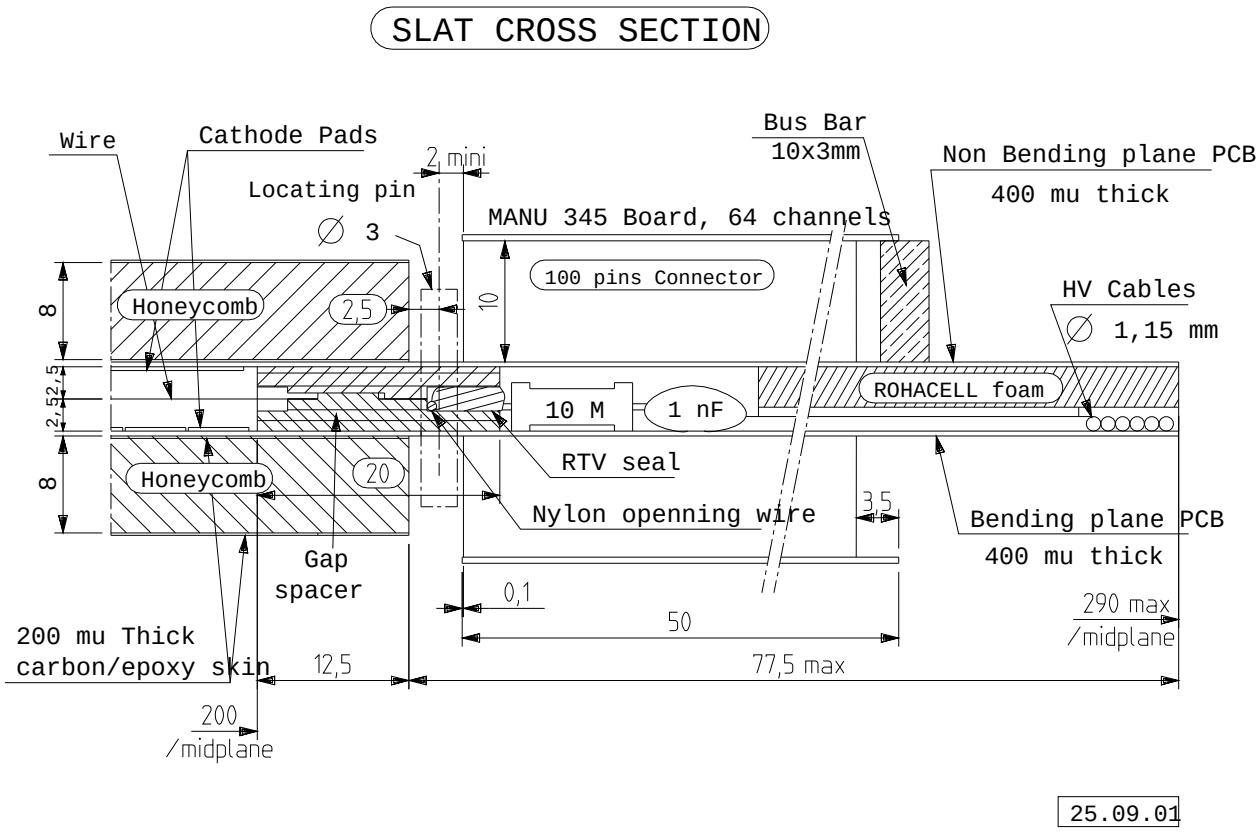

Figure 1. Schematic view of the edge of the CSC slat prototype.

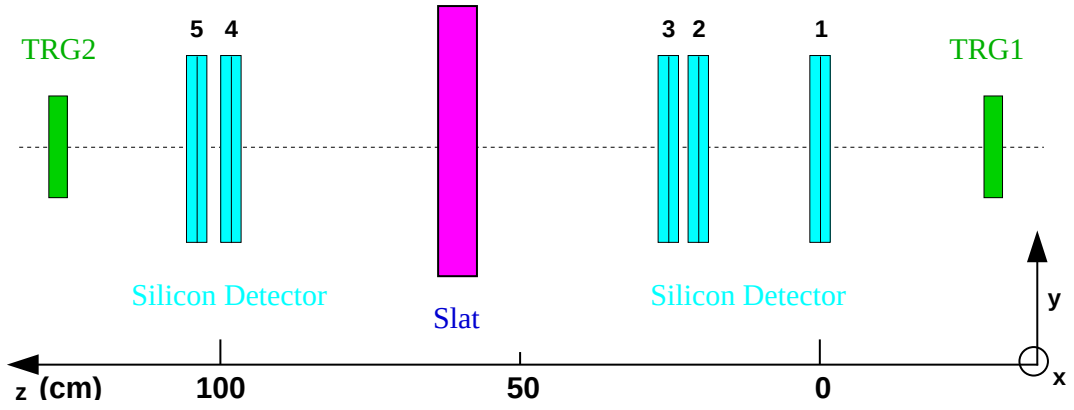

Figure 2. The experimental setup used for the PS beam test in October 2001.

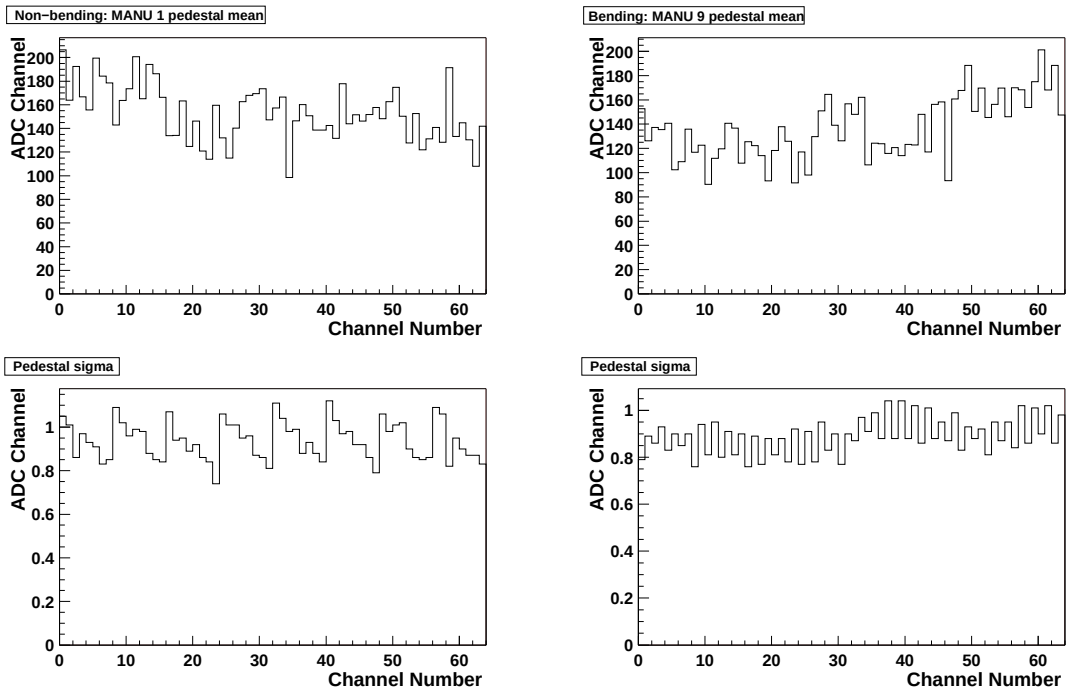

Figure 3. A typical example of mean and sigma pedestal value for the non-bending plane (left side) and for the bending plane (right side).

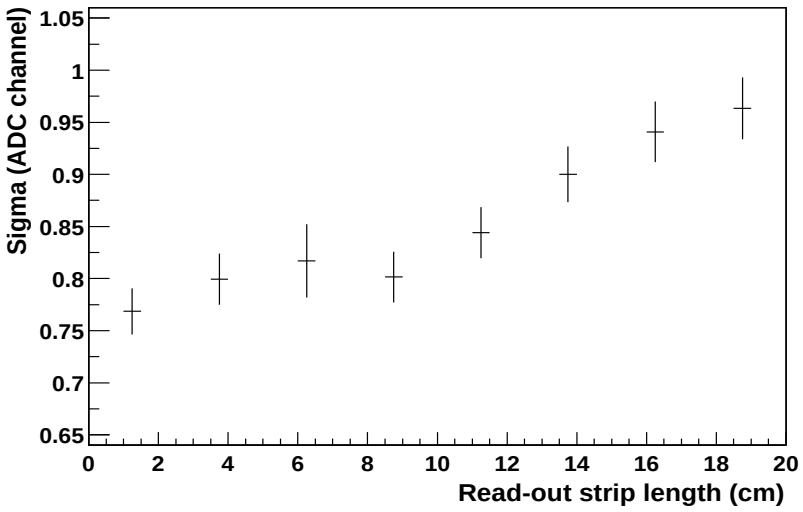

Figure 4. Level of the noise (sigma of the pedestals) versus the length (cm) of the lines connecting pads to the electronics (bending plane).

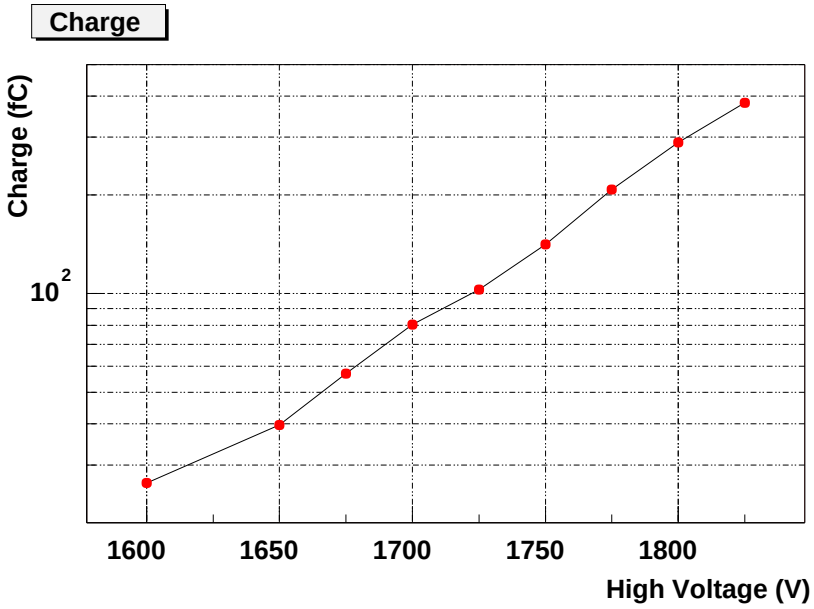

Figure 5. Total cluster charge as a function of the anode high voltage for the bending plane.

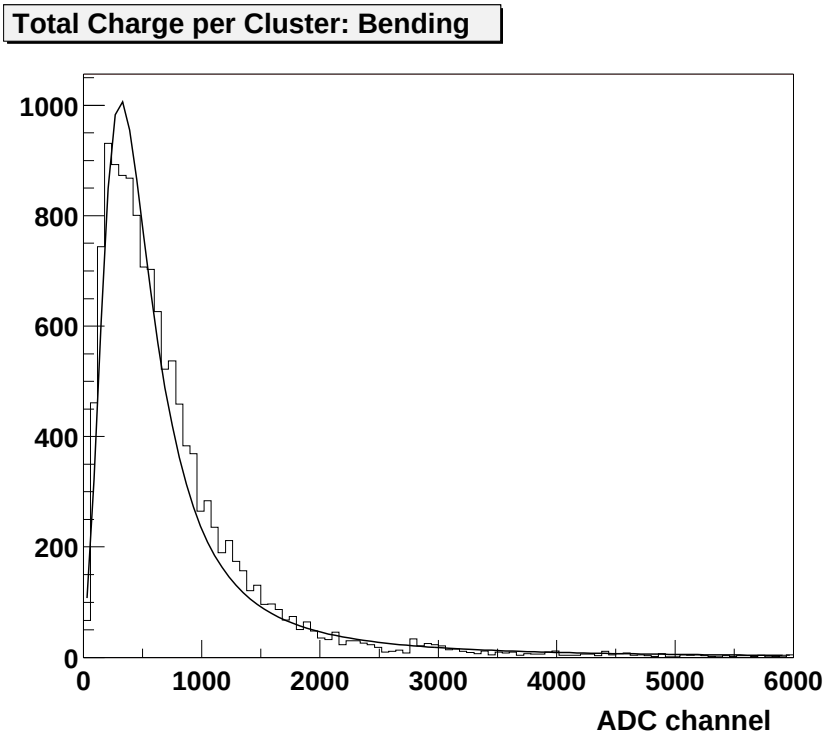

Figure 6. A typical total charge measured in the bending plane at 1750 V. The thick line is the result of a fit using a Landau function.

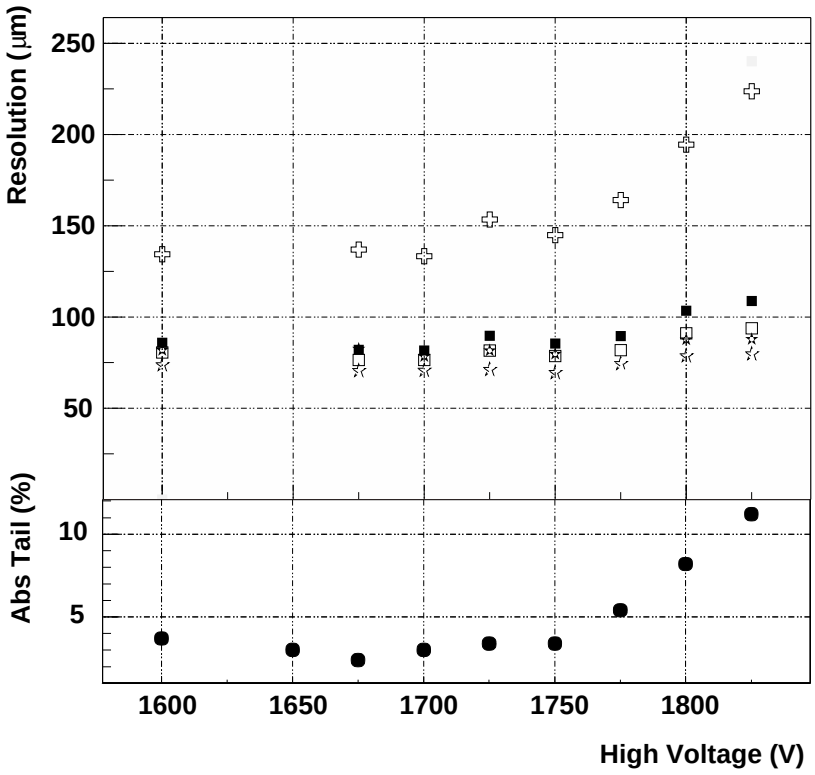

Figure 7. Resolution and amount of events in the tail of the residual distribution for different fitting procedures as a function of applied high voltage for the bending plane: full square symbol stands for a Gaussian fit, the open square symbol stands for a Gaussian fit with weight equal to 1, the full star symbol stands for a double Gaussian fit, the open star symbol stands for double Gaussian fit with weight equal to 1 and the open cross symbol stands for the RMS of the distribution. Due to electronic problems, the results for the 1650 V run are often removed because of a lack of statistics.

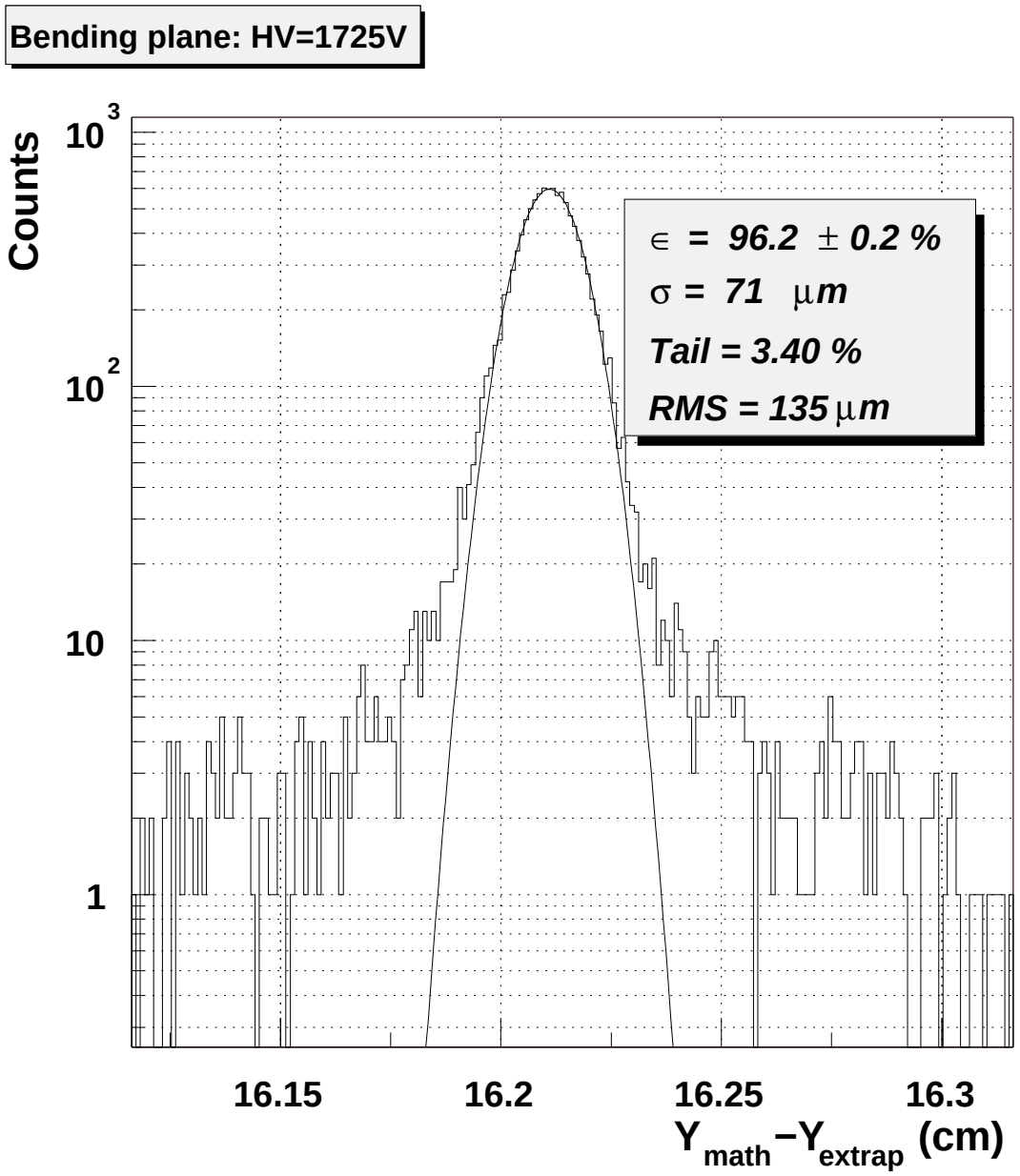

Figure 8. Residuals spectrum for the bending plane at 1725 V applied high voltage. The Gaussian fit procedure is performed in a window of $\pm$ 1 σ.

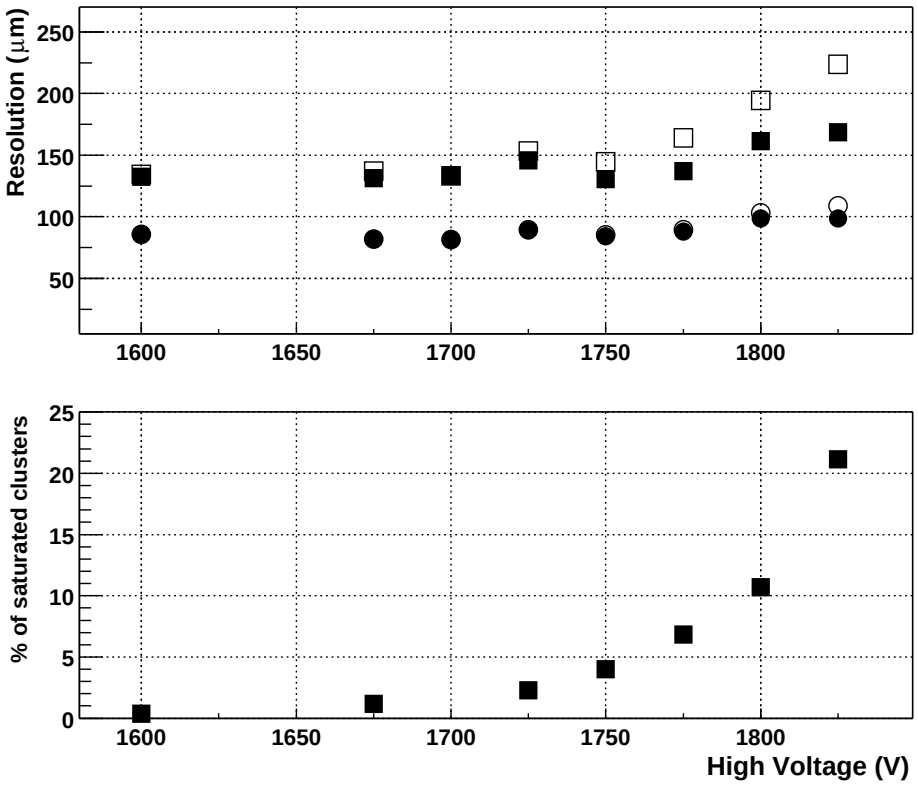

Figure 9. Study of the saturation's effects versus HV. The graph on the top shows the resolution with (open symbols) and without (full symbols) saturations for two different methods (RMS=square and Gauss=circle). The graph on the bottom indicates the percentage of saturated clusters.

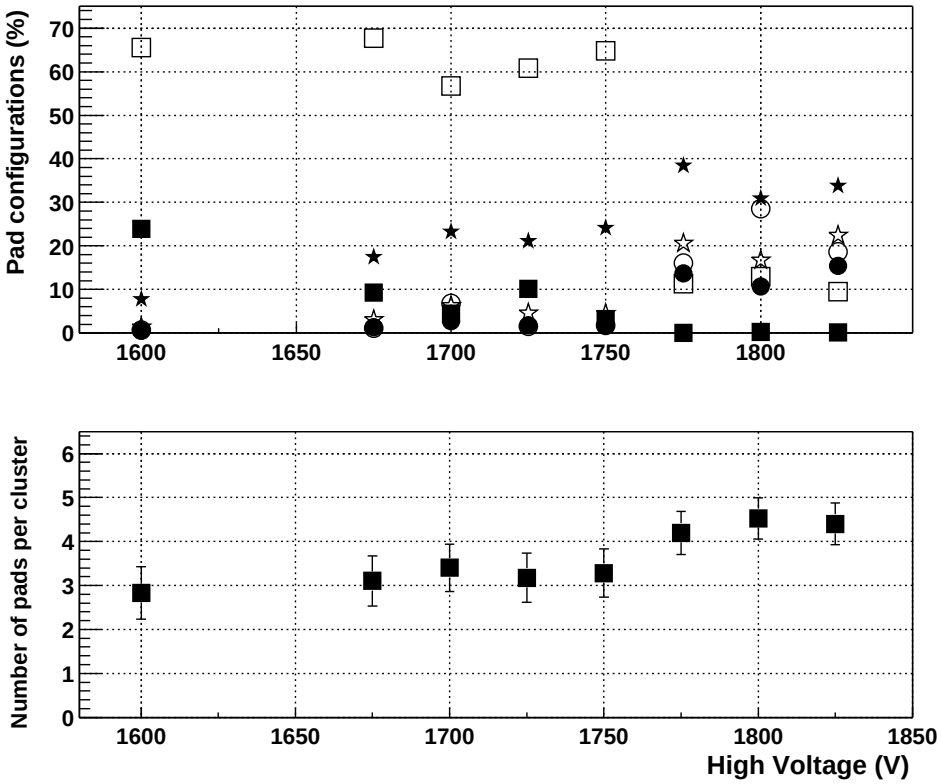

Figure 10. Percentage of clusters with 1 pad up to 6 pads in the y direction versus HV. The graph on the top presents a detailed view (each pad configuration appears with full square symbol for 2 pads, open square symbol for 3 pads, full star symbol for 4 pads, open star symbol for 5 pads, full circle symbol for 6 pads and open circle for more than 6 pads). The bottom panel shows the average number of pads per cluster in the y direction.

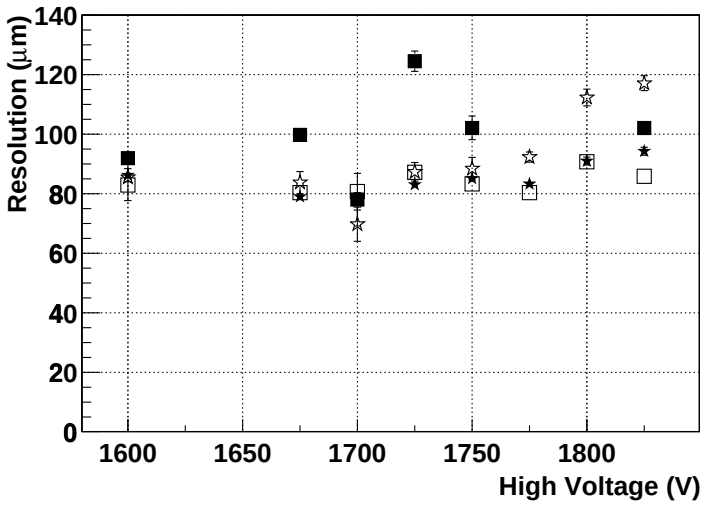

Figure 11. Resolution obtained with a gaussian fit, versus HV for different number of pads hit per cluster: the full square symbol stands for 2 pads hit, the open square symbol stands for 3 pads hit, the full star symbol stands for 4 pads hit and the open star symbol stands for 5 pads hit.

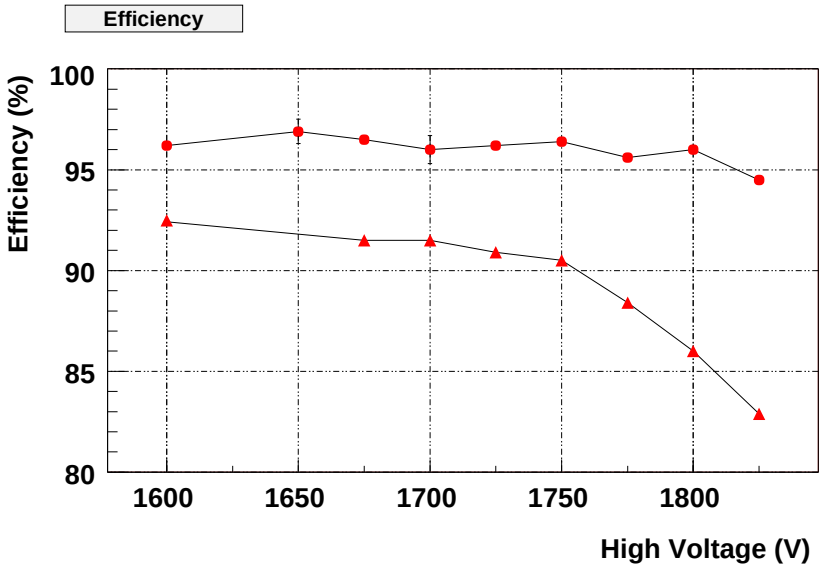

Figure 12. Efficiency as a function of the anode high voltage for the bending plane: the dot symbol represents the ± 1 mm selection and the triangle symbol corresponds to the ± 240 μm selection (3 σ).

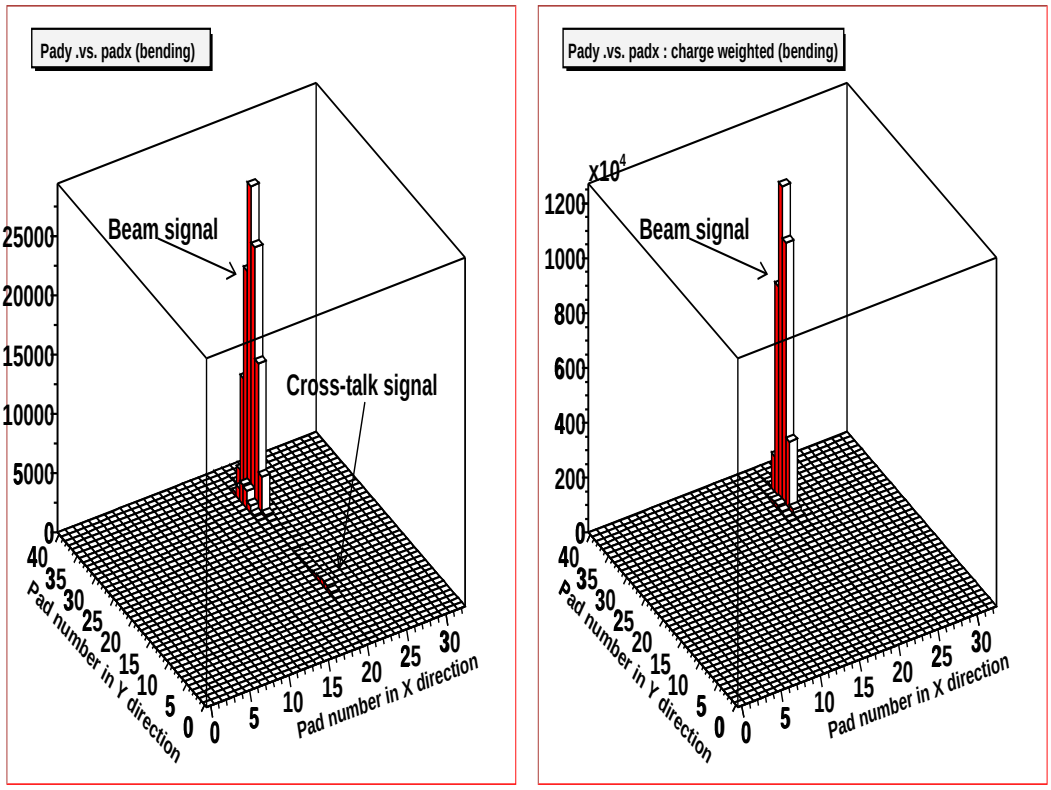

Figure 13. Cross-talk effect: Hits distribution in the bending plane (left), same but charge weighted (right).

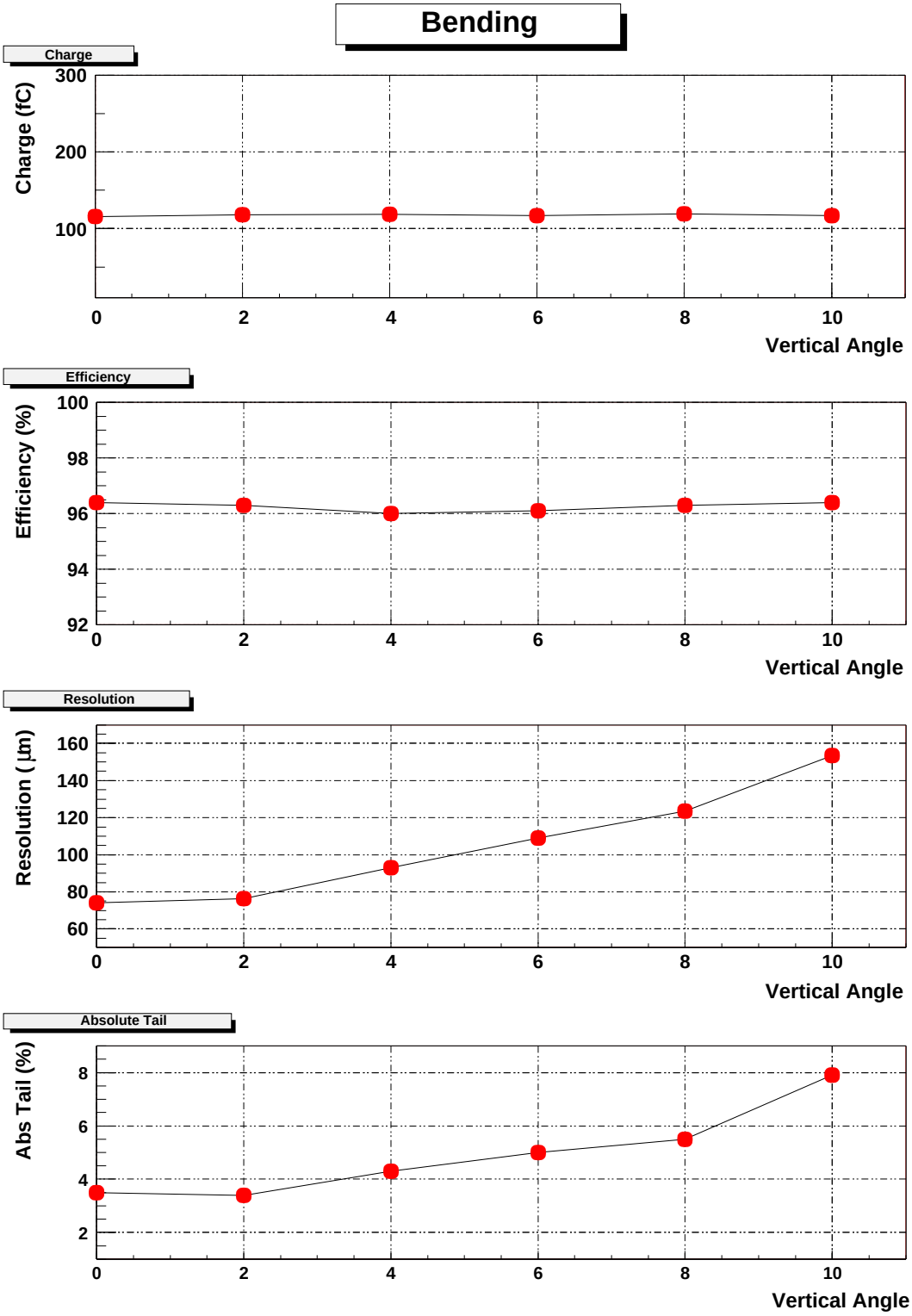

Figure 14. Cluster charge, efficiency (± 1mm), resolution, and absolute tail as a function of the tilt angle with respect to the anode wire for the bending plane. The null value corresponds to normal incidence onto the wire.

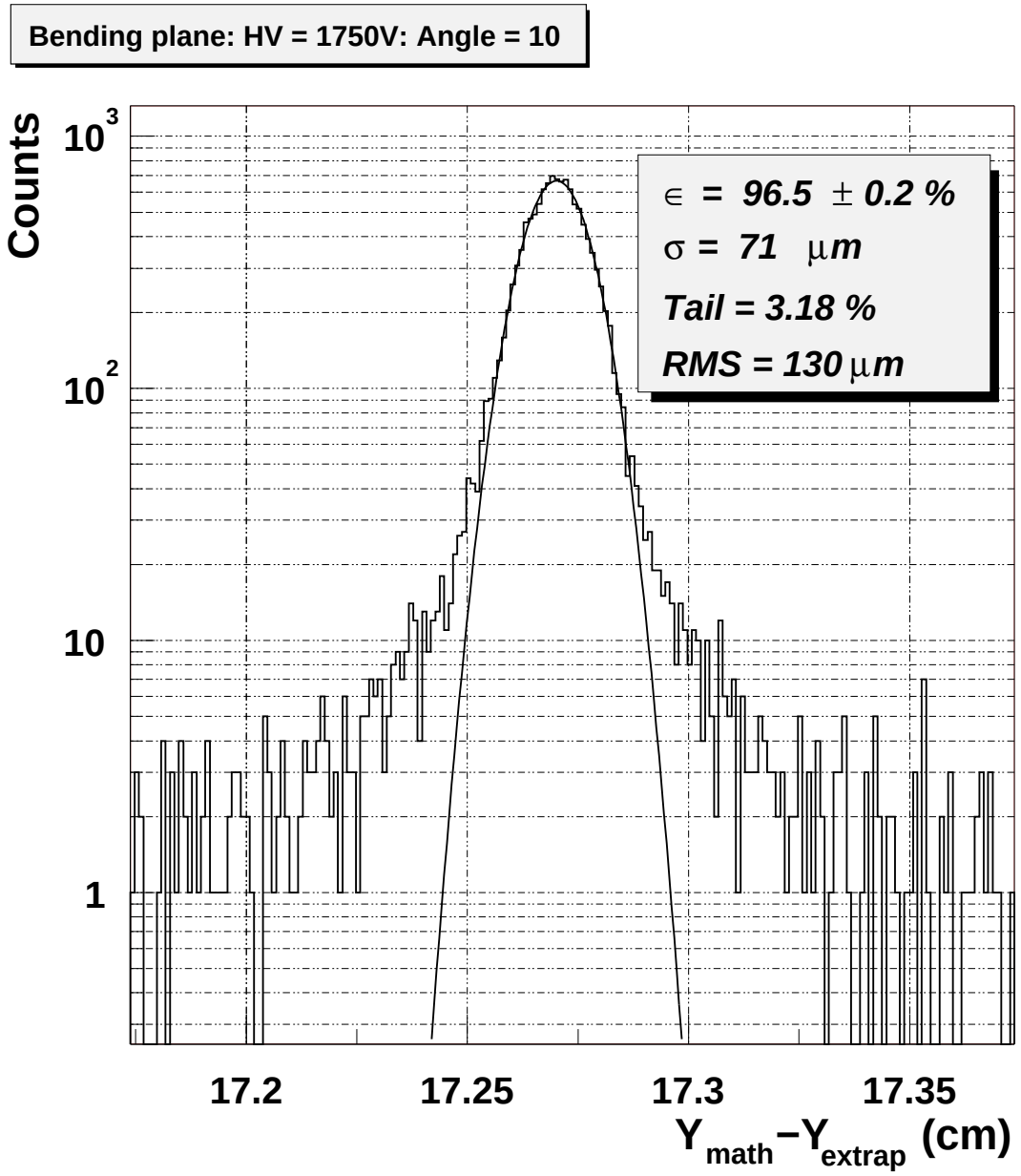

Figure 15. Residuals spectrum for the bending plane at 1750 V applied high voltage and with a rotated position of the slat around the wire axis of 10^o. The Gaussian fit procedure is performed in a window of $\pm$ 1 σ.

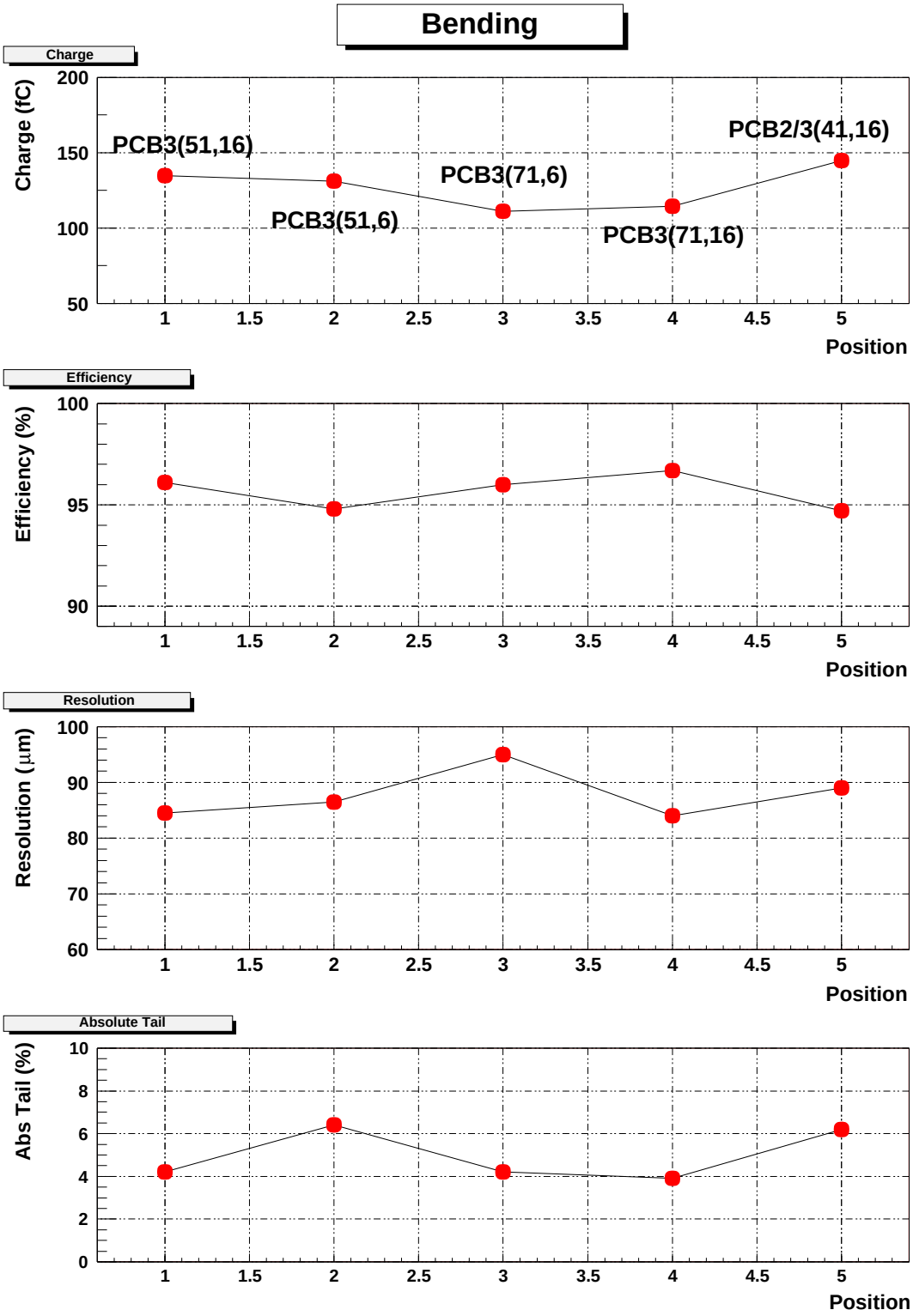

Figure 16. Cluster charge, efficiency (± 1 mm), resolution, and absolute tail measured for different positions on the chamber. The numbers in the brackets on the top panel represent the coordinates in cm with respect to the center of the slat. The acronym PCB stands for printed circuit board and refers to the chamber section number.

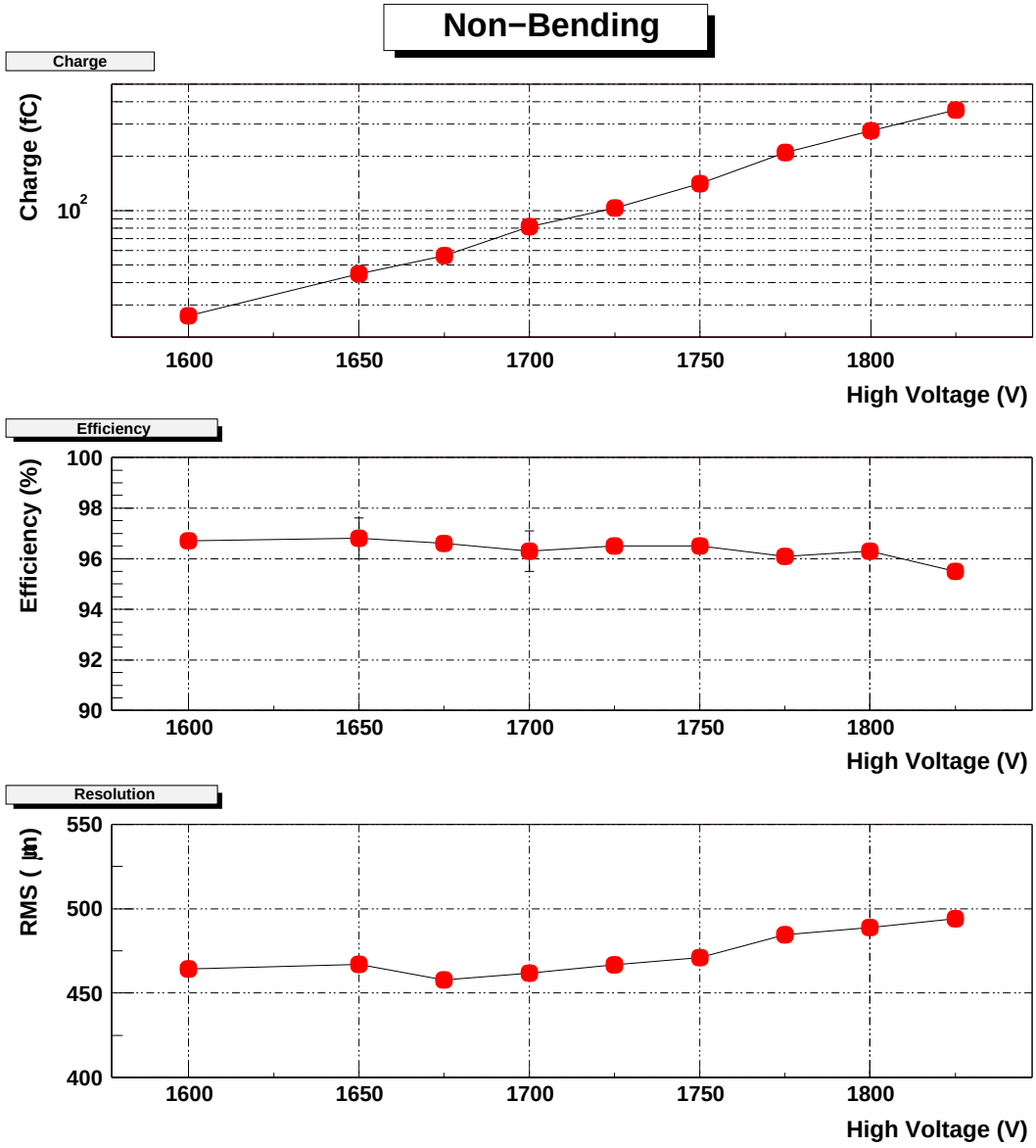

Figure 17. Cluster charge, efficiency (± 1mm), resolution, and absolute tail as a function of applied high voltage for the non-bending plane.

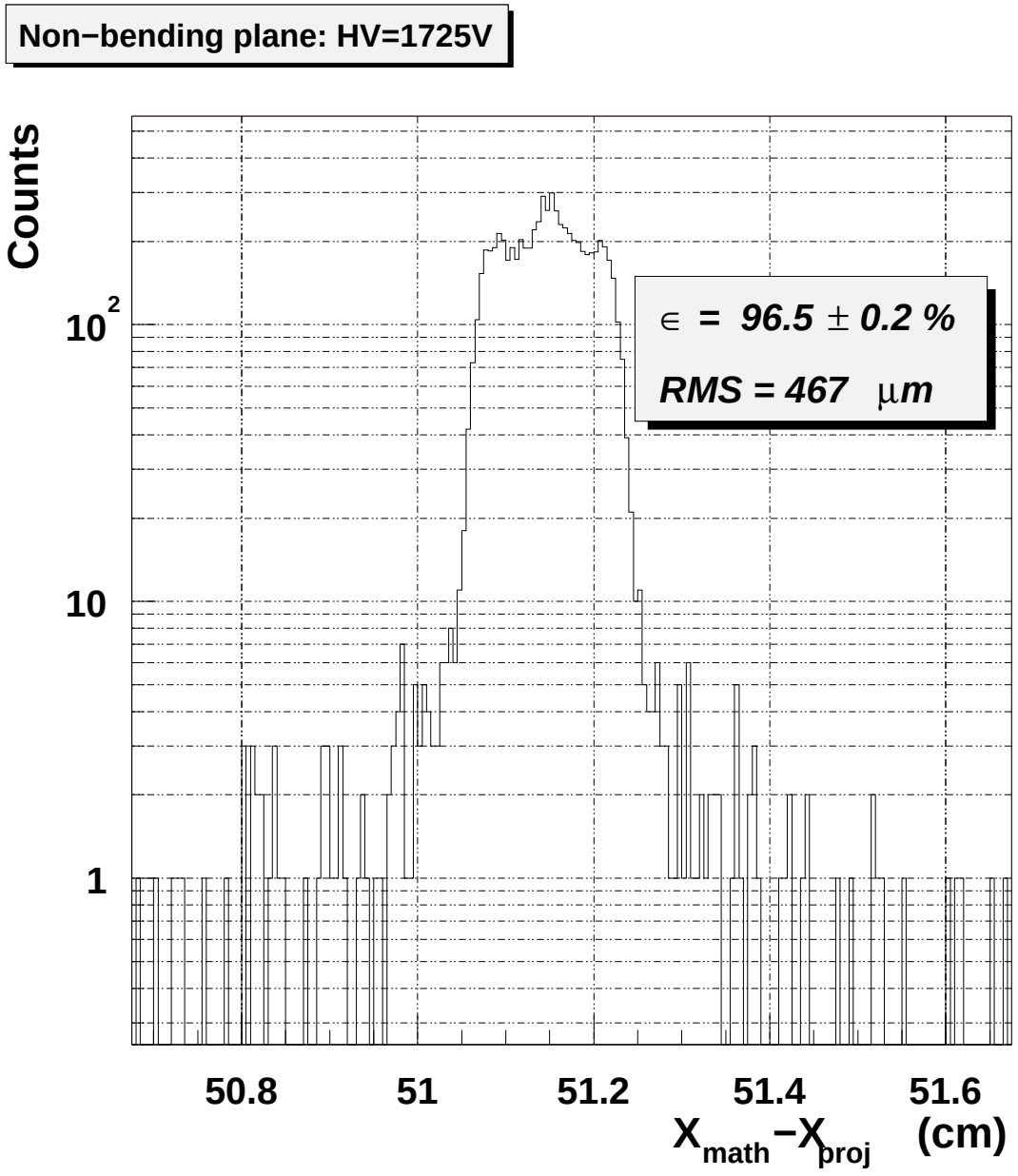

Figure 18. Residuals spectrum for the non-bending plane at 1725 V.

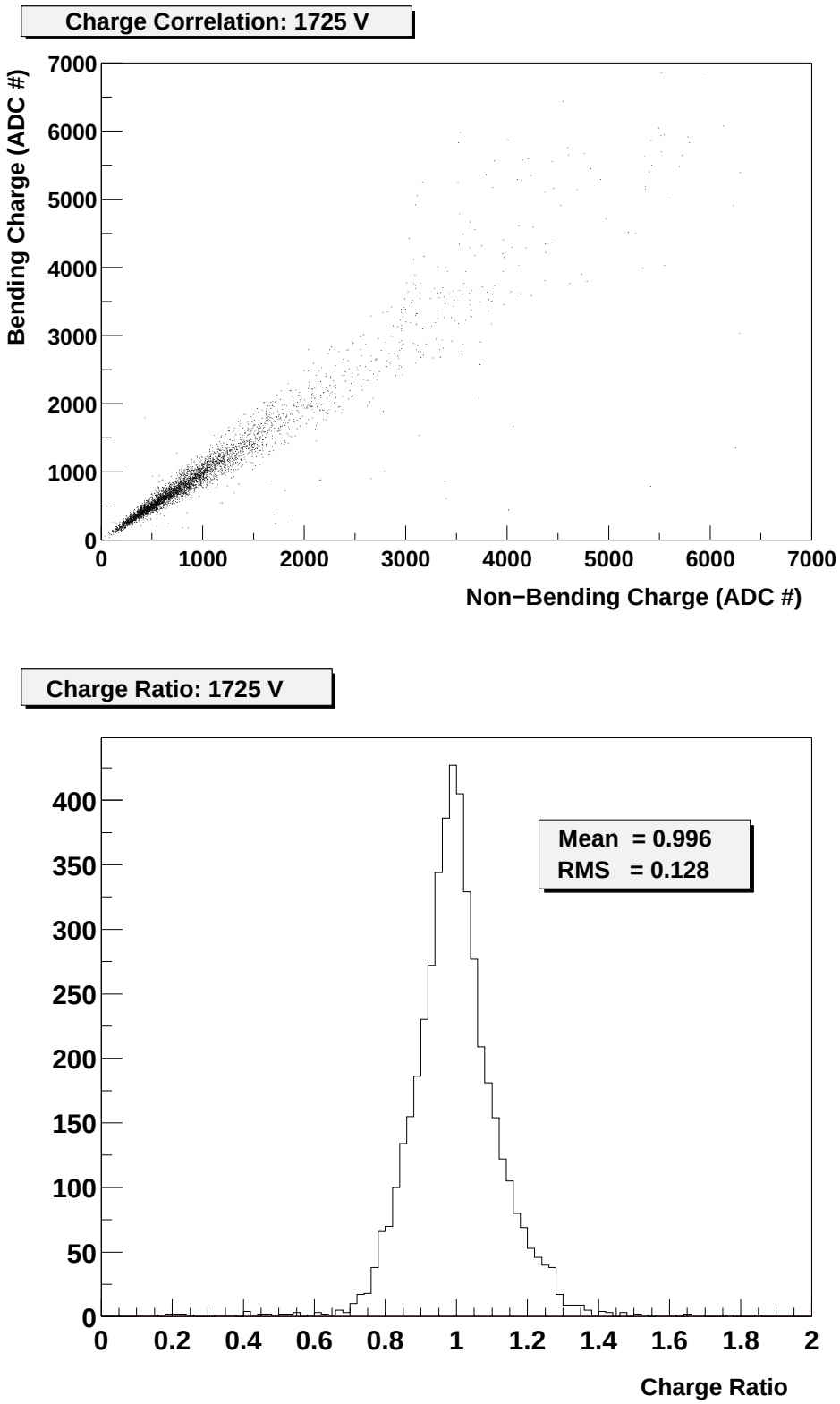

Figure 19. Total cluster charge measured in the bending plane, versus the non-bending plane, in the upper panel. The cluster charge ratio between the two planes (without calibration) is depicted in the lower panel.